Supporting Information

Ultra-high thermally conductive graphite microplatelet/aramid nanofiber composites with reduced interfacial thermal resistances by engineered interface π-π interactions

Yu-Yang Song, Niu Jiang, Shuang-Zhu Li, Lu-Ning Wang, Lu Bai, Jie Yang, Wei Yang**

College of Polymer Science and Engineering, Sichuan University, State Key Laboratory of Polymer Materials Engineering, Chengdu 610065, Sichuan, P. R. China

*Corresponding authors: psejieyang@scu.edu.cn (J. Yang); weiyang@scu.edu.cn (W. Yang); Fax: +86 28 8546 0130; Tel: +86 288546 0130

Supplementary Figures and Tables

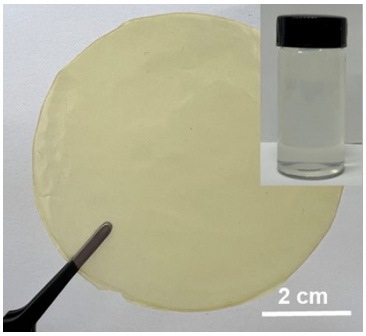

Figure S1. Digital photos of the ANF film and the ANF/DMSO/DI dispersion.

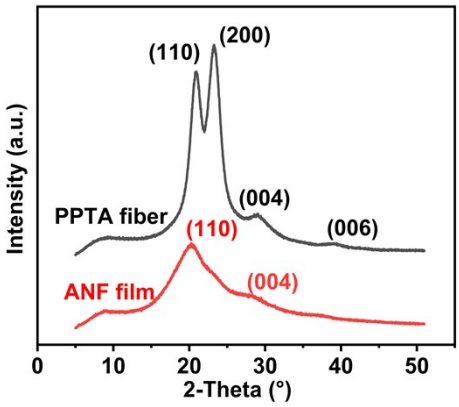

Figure S2. XRD patterns of pristine PPTA fiber and ANF film.

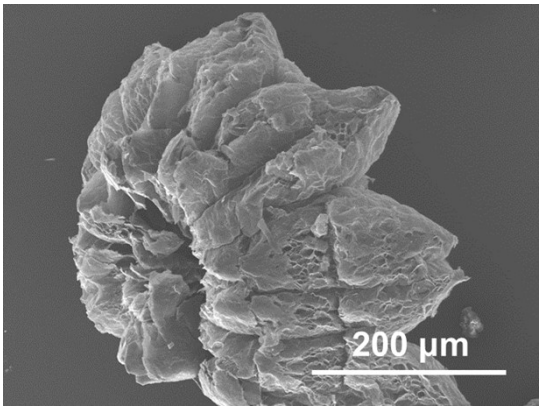

Figure S3. SEM image of pristine EG.

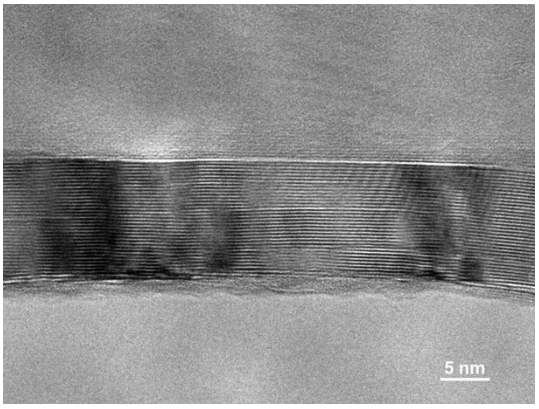

Figure S4. TEM image of F-GMP.

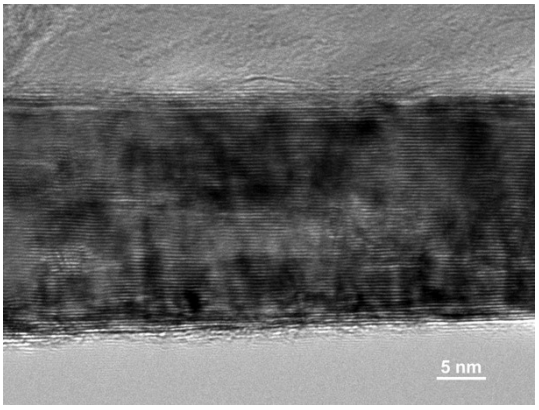

Figure S5. TEM image of GMP.

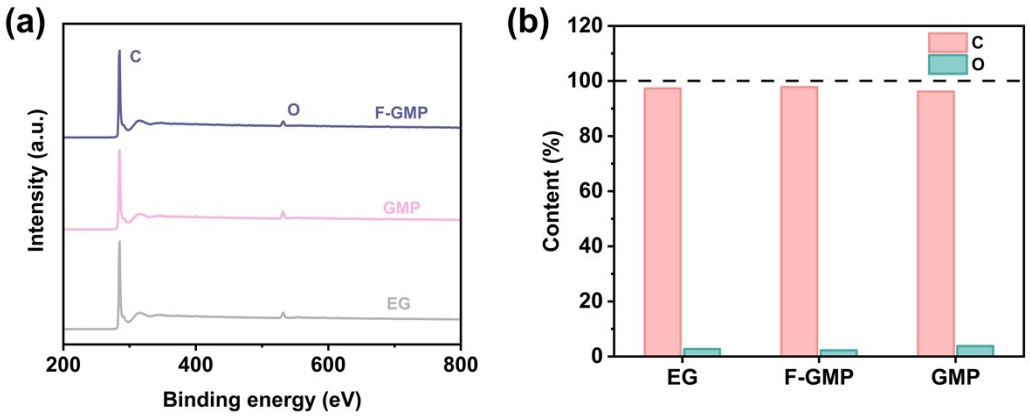

Figure S6. (a) XPS spectra of pristine EG, F-GMP, and GMP. (b) Oxygen and carbon contents in EG, F-GMP, and GMP.

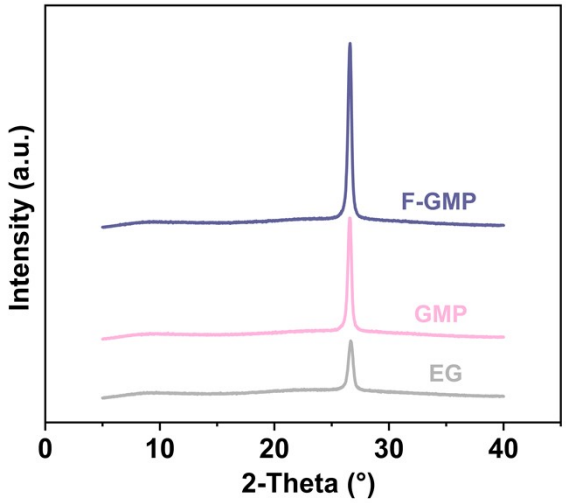

Figure S7. XRD patterns of pristine EG, F-GMP, and GMP.

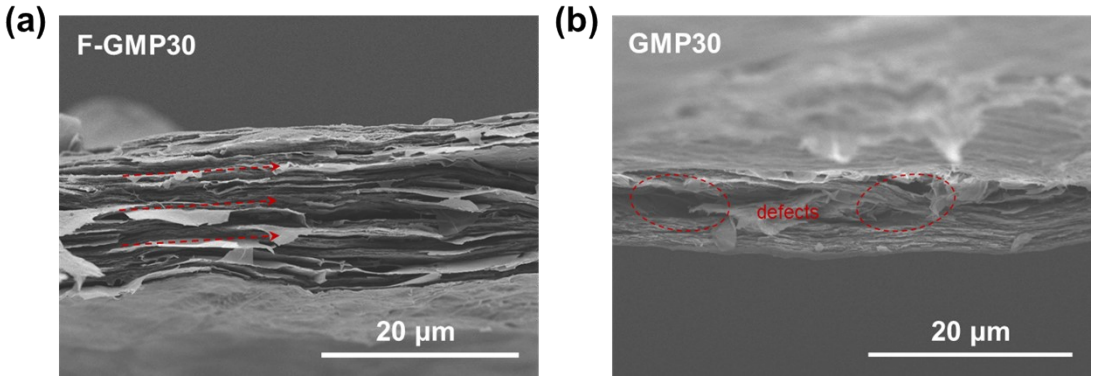

Figure S8. Cross-sectional SEM images of the (a) F-GMP30 and (b) GMP30 composite films.

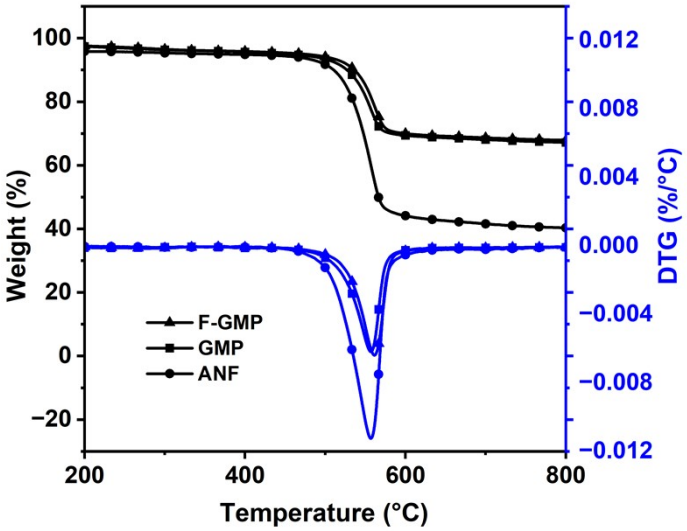

Figure S9. TGA and DTG curves of ANF, F-GMP and GMP composite films.

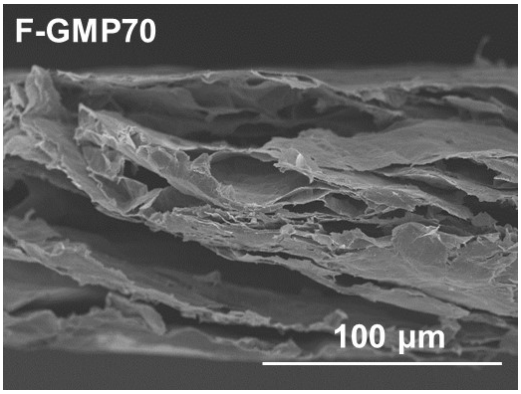

Figure S10. Cross-sectional SEM image of the F-GMP70 composite film.

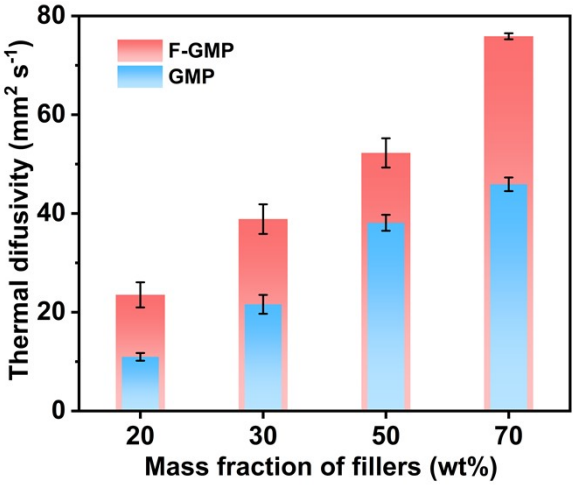

Figure S11. In-plane thermal diffusivity of the composite films.

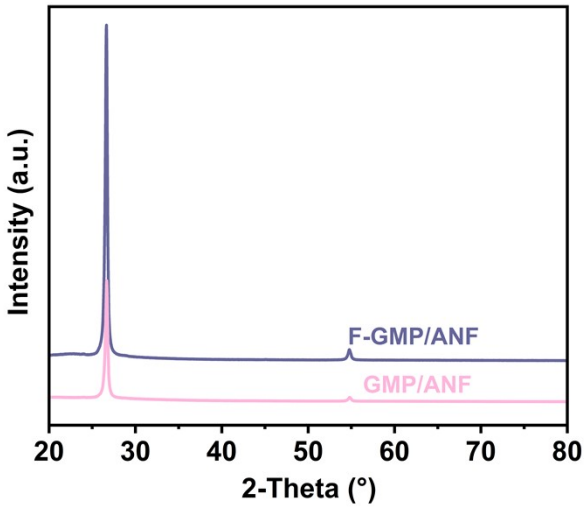

Figure S12. XRD patterns of the F-GMP/ANF and GMP/ANF composite films.

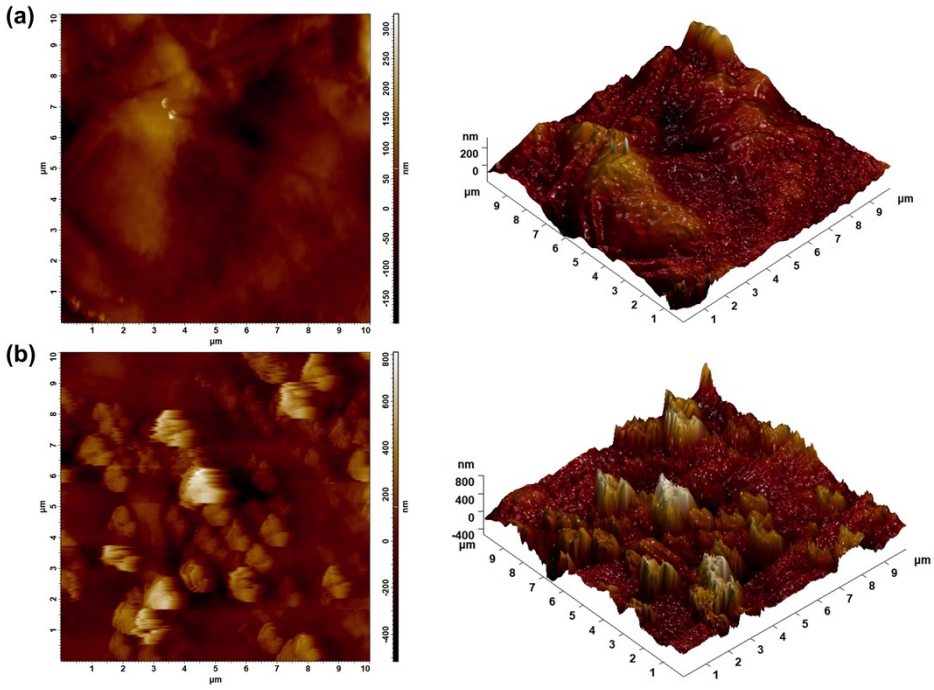

Figure S13. AFM images of (a) F-GMP/ANF and (b) GMP/ANF composite films.

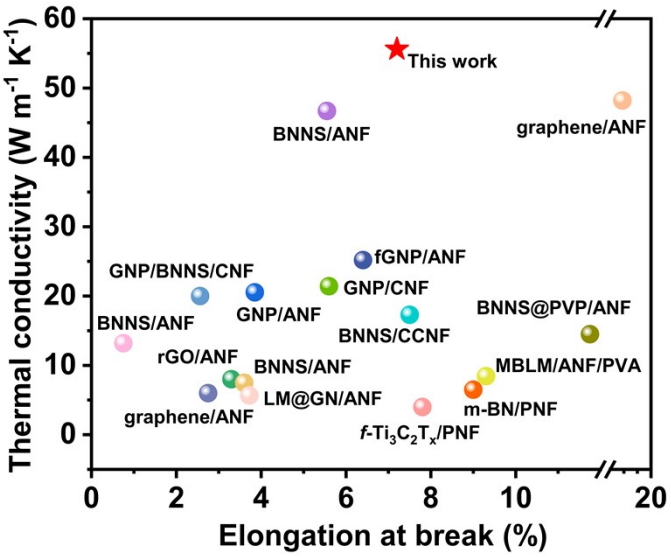

Figure S14. A comparison of the thermal conductivity and the elongation at break between the composite films developed in this work and previously-reported nanofiber-based thermally conductive composite films [S1-16].

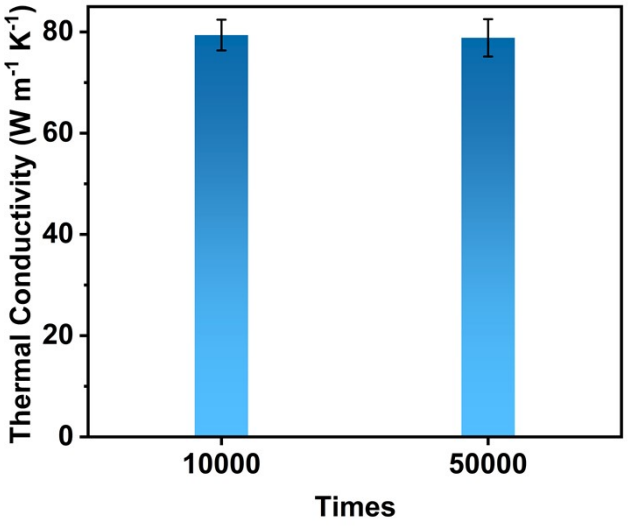

Figure S15. Thermal conductivity variation of the F-GMP70 composite film after bending for 10, 000 and 50, 000 times.

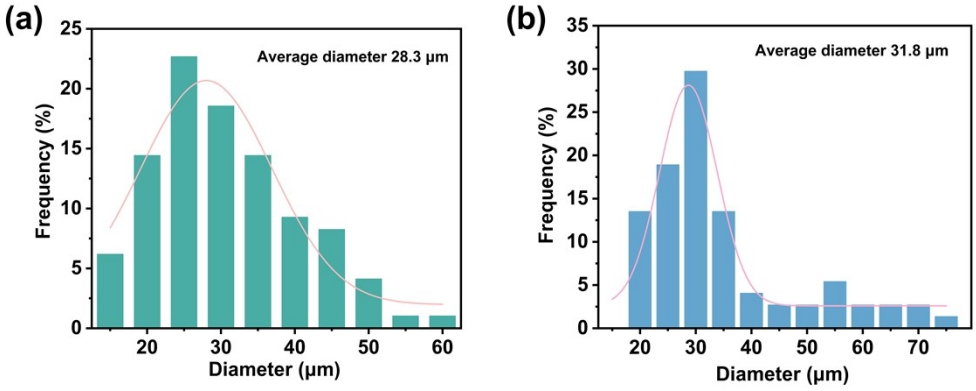

Figure S16. Dimensional statistics of (a) F-GMP and (b) GMP.

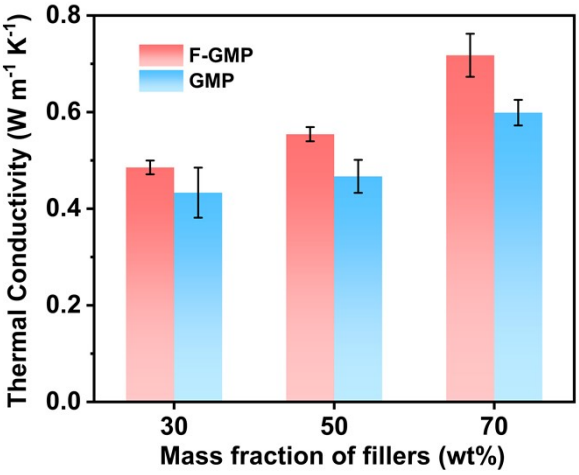

Figure S17. Through-plane thermal conductivity of the composite films.

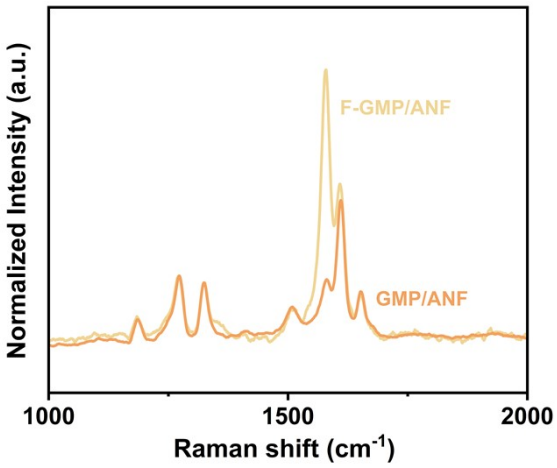

Figure S18. Normalized Raman spectra of F-GMP/ANF and GMP/ANF composite films.

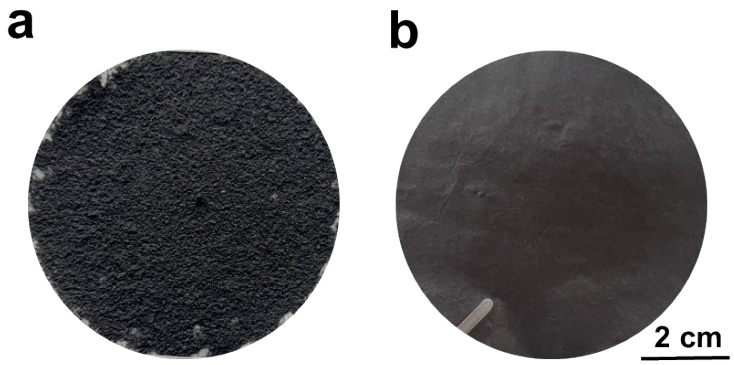

Figure S19. Digital photos of the composite films prepared from (a) GMP/ANF and (b) F-GMP/ANF pastes after the long-term storage for 7 days.

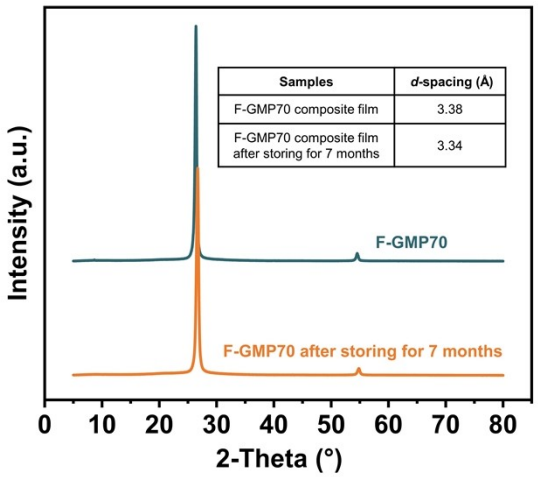

Figure S20. XRD patterns of the F-GMP70 composite film before and after storing for 7 months.

Table S1. Density and porosity of the F-GMP/ANF and GMP/ANF composite films.

Samples	Density (g/cm^3)	Porosity (%)
F-GMP20	1.20	20.3
GMP20	1.01	32.9
F-GMP30	1.22	24.1
GMP30	0.95	40.9
F-GMP50	1.13	37.4
GMP50	0.87	51.8
F-GMP70	1.05	46.5
GMP70	0.87	55.7

Table S2. Average surface roughness of the F-GMP/ANF and GMP/ANF composite films.

Samples	Roughness average (nm)
F-GMP/ANF	37.3
GMP/ANF	128.9

Table S3. A comparison of the thermal conductivity, thermal conductivity enhancement efficiency and elongation at break of F-GMP/ANF composite films with the previously-reported thermally conductive composite films.*

Materials	Content of fillers (wt%)	Thermal conductivity (W m^{-1} K^{-1})	Thermal conductivity enhancement efficiency (%)	Elongation at break (%)	Refs.
GNP/ANF	30	25.2	34.8	6.4	[S1]
GNP/ANF	20	20.54	\	~3.85	[S2]
rGO/ANF	30	~8	\	~3.3	[S3]
Graphene/ANF	40	48.2	\	18.6	[S4]
BNNS/ANF	30	46.7	\	5.55	[S5]
BNNS/ANF	30	7.5	9.2	3.6	[S6]
BNNS/ANF	28	0.75	\	~13.2	[S7]
Graphene/ANF	30	6	12.7	2.75	[S8]
BNNS@PVP/ANF	40	14.5	13.5	11.75	[S9]
BNNS/ANF -AgNWs@BNNS-BNNS/ANF (BAB)	30	~8	21.6	25.5	[S17]
s-IL@BNNS/ANF	30	~16	8.5	\	[S18]
LM@GN/ANF	32.5	5.67	11.5	3.72	[S10]
MBLM/ANF/PVA	75	8.45	\	9.3	[S11]
IL@BNNS/ANF	40	15.2	3.3	22.3	[S19]
m-BN/PNF	30	~6.5	5.3	~9	[S12]
MXene/PNF	30	~41	2	~30	[S20]
f-$Ti_3C_2T_x$/PNF	30	~4	2	~7.8	[S13]

GNP/BNNS/CNF	30	~20	6.9	~2.56	[S14]
GNP/CNF	40	21.42	51.1	~5.6	[S15]
BNNS/CCNF	50	17.3	67.2	~7.5	[S16]
BNNS-OH@CNF	30	~5.8	10.5	\	[S21]
LM/CNF	85	4.9	1.9	5.5	[S22]
Al_2O_3-NH_2/MXene/BC	40	20.02	10.9	\	[S23]
F-GMP/ANF	**30**	**56.89**	**33.4**	**7.2**	**This work**

*GNP: graphene nanoplatelet, rGO: reduced graphene oxide, BNNS: boron nitride nanosheet, PVP: polyvinylpyrrolidone, AgNWs@BNNS: hetero-structured silver nanowires@boron nitride nanosheets, s-IL@BNNS: sulfonated ionic liquid modified BNNSs, MBLM: MXene-bridging-liquid metal, PVA: polyvinyl alcohol, *m*-BN: benzidine-functionalized boron nitride, *f*-$Ti_3C_2T_x$: polyetherimide-unctionalized $Ti_3C_2T_x$, PNF: poly(*p*-phenylene benzobisoxazole) nanofiber, BNNS-OH: hydroxylated boron nitride nanosheets, CNF: cellulose nanofiber, CCNF: carboxymethylated CNF, Al_2O_3-NH_2: ammoniated alumina, BC: bacterial cellulose.

Table S4. Mass and volume fractions of thermally conductive fillers in the composite films.

Samples	Mass fraction (wt%)	Volume fraction (vol%)
F-GMP70/GMP70	70	60.4
F-GMP50/GMP50	50	39.6
F-GMP30/GMP30	30	21.9
F-GMP20/GMP20	20	14.1

Table S5. Parameters for the calculation of interfacial thermal resistance.

Samples	Thickness of graphite (nm)	Effective length of graphite (μm)
F-GMP	11.7	28.3
GMP	22.7	31.8

Supplementary References

S1. M. C. Vu, P. J. Park, S.-R. Bae, S. Y. Kim, Y.-M. Kang, W. K. Choi, M. A. Islam, J. C. Won, M. Park and S.-R. Kim, *J. Mater. Chem. A*, 2021, **9**, 8527-8540.

S2. X. He, K. Zhang, H. Wang, Y. Zhang, G. Xiao, H. Niu and Y. Yao, *Carbon*, 2022, **199**, 367-378.

S3. M. Yan, X. Chen, Y. Xu, Y. Pan, J. Li, J. Li, T. Wu, H. Zheng, X. Chen and J. He, *Compos. Commun.*, 2023, **37**, 101428.

S4. L. Huang, G. Xiao, Y. Wang, H. Li, Y. Zhou, L. Jiang and J. Wang, *Nano-Micro Lett.*, 2022, **14**, 168.

S5. K. Wu, J. Wang, D. Liu, C. Lei, D. Liu, W. Lei and Q. Fu, *Adv. Mater.*, 2020, **32**, 1906939.

S6. L.-H. Zhao, L. Wang, Y.-F. Jin, J.-W. Ren, Z. Wang and L.-C. Jia, *Composites, Part B*, 2022, **229**, 109454.

S7. R. Tian, X. Jia, M. Lan, J. Yang, S. Wang, Y. Li, D. Shao, L. Feng and H. Song, *Chem. Eng. J.*, 2022, **446**, 137255.

S8. D. K. Nguyen, T. T. H. Tran, T. K. L. Mai, M.-S. Tran, S. Ghotekar, A. L. H. Pham, V.-C. Nguyen and M. C. Vu, *ACS Appl. Nano Mater.*, 2023, **7**, 2724-2734.

S9. J. Ren, G. Jiang, Z. Wang, Q. Qing, F. Teng, Z. Jia, G. Wu and S. Jia, *Adv. Compos. Hybrid Mater.*, 2023, **7**, 5.

S10. W. Luo, B. Wei, T. Luo, B. Li and G. Zhu, *Small*, 2024, **20**, 2406574.

S11. Y. Sun, Y. Su, Z. Chai, L. Jiang and L. Heng, *Nat. Commun.*, 2024, **15**, 7290.

S12. L. Tang, K. Ruan, X. Liu, Y. Tang, Y. Zhang and J. Gu, *Nano-Micro Lett.*, 2023, **16**, 38.

S13. L. Wang, Z. Ma, Y. Zhang, H. Qiu, K. Ruan and J. Gu, *Carbon Energy*, 2022, **4**, 200-210.

S14. J. Yun, J. Lee, J. Kim, J. Lee and W. Choi, *Carbon*, 2024, **228**, 119397.

S15. B. Zhang, L. Wang, C. Zhang and S. Wu, *Chem. Eng. J.*, 2022, **439**, 135675.

S16. K. Chen, L. Peng, Z. Fang, X. Lin, C. Sun and X. Qiu, *Carbohydr. Polym.*, 2023, **321**, 121250.

S17. Y. Han, K. Ruan, X. He, Y. Tang, H. Guo, Y. Guo, H. Qiu and J. Gu, *Angew. Chem. Int. Ed.*, 2024, **63**, e202401538.

S18. X. Li, B. Wu, Y. Lv, R. Xia and J. Qian, *Chem. Eng. J.*, 2025, **503**, 158246.

S19. X. Li, B. Wu, Y. Lv, R. Xia and J. Qian, *J. Mater. Chem. A*, 2024, **12**, 864-875.

S20. Y. Liu, W. Zou, N. Zhao and J. Xu, *Nat. Commun.*, 2023, **14**, 5342.

S21. Y. Liao, D. Wang, M. Ma, S. Chen, Y. Shi, H. He, Y. Zhu and X. Wang, *Composites, Part B*, 2025, **295**, 112197.

S22. N. Ren, Y. Ai, N. Yue, M. Cui, R. Huang, W. Qi and R. Su, *ACS Appl. Mater. Interfaces*, 2024, **16**, 17904-17917.

S23. C. Wang, Z. Zhao, S. Zhou, L. Wang, X. Liu and R. Xue, *J. Mater. Sci. Technol.*, 2025, **213**, 162-173.